Received 28 February 2021; accepted 19 March 2021. Date of publication 23 March 2021; date of current version 1 April 2021.

Digital Object Identifier 10.1109/OJCOMS.2021.3068144

Performance of Multiple Relay DF NLOS UVC System With CSI Imperfections

KAMAL K. GARG [1], PARVEZ SHAIK [1] (Graduate Student Member, IEEE), PRAVEEN K. SINGYA [2] (Member, IEEE), AND VIMAL BHATIA [1] (Senior Member, IEEE)

[1]Department of Electrical Engineering, Indian Institute of Technology Indore, Indore 453552, India

[2]Computer, Electrical, and Mathematical Science and Engineering Division, King Abdullah University of Science and Technology, Thuwal 23955, Saudi Arabia

CORRESPONDING AUTHOR: KAMAL K. GARG (e-mail: phd1701102008@iiti.ac.in)

This work was supported in part by the Ministry of Electronics and Information Technology Research and Development Work, Government of India, through the Visvesvaraya Ph.D. Scheme being implemented by Digital India Corporation.

ABSTRACT Ultraviolet communication (UVC) is emerging as an attractive alternative to the existing optical wireless communication (OWC) technologies. UVC experiences negligible noise on the earth's surface, and also has the ability to operate in non-line-of-sight (NLOS) mode, thereby making it a perfect choice for outdoor communication. However, due to strong interaction of ultraviolet waves with atmospheric particles, it suffers from a very high path loss and turbulence-induced fading, which limits UVC system's performance. We consider a decode-and-forward based cooperative relaying technique to improve the performance of NLOS UVC system, and to extend its communication range. We consider the practical case of imperfect channel state information at the receiver and derive outage probability of the system. We also consider impact of elevation angles, receiver field-of-view (FOV), and turbulence strength on the system performance. We compute the relative diversity order of the system and demonstrate its convergence through asymptotic analysis. Next, we obtain the novel expression of probability density function of the end-to-end instantaneous signal-to-noise-ratio. We use single subcarrier intensity modulation employing quadrature amplitude modulation (QAM) and derive the novel generalized analytical expressions for rectangular QAM, cross QAM, and futuristic hexagonal QAM schemes. We carry out a detailed performance study considering different system configurations and several interesting insights are highlighted, which reinforces UVC as a futuristic OWC technology. Correctness of the derived analytical expressions is confirmed using Monte-Carlo simulations.

INDEX TERMS NLOS UVC, decode-and-forward (DF), outage probability, average symbol error rate (ASER), quadrature amplitude modulation (QAM), cross QAM (XQAM), hexagonal QAM (HQAM).

I. INTRODUCTION

ULTRAVIOLET communication (UVC) is attracting renewed research attention due to advancement in solid-state technologies and myriad applications [1] specifically in the non-line-of-sight (NLOS) communication systems. UVC, with its ability to communicate in NLOS mode offers several significant advantages such as high security, availability of abundant unlicensed spectrum; and relaxed pointing, acquisition, and tracking (PAT) requirements. The popular deep UV band (also known as UV-C band) with a wavelength (range) of $200-280$ nm is having negligible background noise on the earth's surface due to its absorption by the ozone layer [2]. Hence, NLOS UVC with its versatile nature and unique abilities has become a popular candidate for the future wireless communication systems as compared to other optical wireless communication (OWC) technologies. NLOS UVC is mainly useful in scenarios where line-of-sight (LOS) is not possible to achieve, RF communication is prohibited, and/or security is of paramount importance. In such cases, the conventional OWC technologies such as FSO and VLC can not be used as they impose strict LOS and PAT constraints for their operation. Some of the applications of NLOS UVC includes lidar, aircraft landing aid, military/battlefield etc. [2]. Further, in a recent study it has been found that UV wavelength of 222 nm effectively kills covid-19 virus [3].

In terms of safety, humans are sensitive to the UV radiations and therefore UVC should adhere to the safety standards and threshold limit value (TLV) of the exposure established by International Commission on Non-Ionizing Radiation Protection (ICNIRP) [4] and American Conference of Governmental Industrial Hygienists (ACGIH) [5]. TLV is defined as the condition where nearly all operators may repeatedly be exposed to the ultraviolet radiations, day after day, over a working lifetime, without adverse health effects. The communication in the UV band can safely be carried out by using the transmit power levels conforming to these safety regulations and limits [1], [2], [5].

The NLOS UVC suffers from a very high path loss and turbulence-induced fading, due to its strong interaction with the molecules and aerosols present in the atmosphere. These impairments result in degraded system performance and limit the communication range of NLOS UVC to a short distance [2]. To mitigate this drawback extensive research studies were carried out to develop power efficient long range NLOS UVC system. Cooperative diversity has shown be an effective and proven technique in radio-frequency (RF) communication systems for mitigating the effect of fading and improving the system performance. It is worth mentioning that the outcome of cooperative relaying techniques applied in RF and visible light communication (VLC) systems [6], [7] are not pertinent to UVC due to very different nature and statistical modelling of the NLOS UVC channel. Recently, cooperative relaying has drawn attention of the researchers working in NLOS UVC to further increase the communication range. As a result, there have been several recent studies in which cooperative relaying techniques are used to improve performance of the NLOS UVC systems by combating the effect of turbulence induced fading, and making it suitable for long distance communication [8]–[15]. In [8], Ardakani *et al.* studied the performance of a serial relayed NLOS UVC system considering binary pulse position modulation (BPPM) and weak atmospheric turbulence modeled using lognormal distribution. Authors computed the outage probability and diversity order assuming perfect knowledge of the channel state information (CSI) at the receiver (Rx) nodes. In [9], Ardakani and Uysal proposed a three-node dual-hop cooperative NLOS UVC system ignoring the effect of atmospheric turbulence under the assumption of short-distance link. A frequency selective UVC channel is considered, and DC-biased optical orthogonal frequency division multiplexing (DCO-OFDM) scheme is used to mitigate the inter-symbol interference (ISI). Authors studied the BER performance of DCO-OFDM in the absence of fading and optimized the source and relay node's power allocation. Further, the system throughput is maximized using bit loading. In [10], Arya and Chung considered strong turbulence scenarios and derived outage probability of a system with multiple correlated Rx branches. In [11], the performance of a multi-relay NLOS UVC system is studied in terms of outage probability assuming the perfect knowledge of CSI. Further, the important performance metrics such as diversity order and average symbol error rate (ASER) are not computed in this work. In [12], authors conducted a detailed performance study of single-input-multiple-output (SIMO) NLOS UVC system under weak turbulence scenarios. Further, the authors derived outage probability, ASER for higher-order quadrature amplitude modulation (QAM) schemes. The performance of a multihop amplify-and-forward (AF) relayed NLOS UVC system is studied in [13] considering the subcarrier intensity modulation (SIM) scheme. In [14], authors considered a parallel dual-hop AF-relayed NLOS UVC system, and evaluated the lower-bound on the outage probability and ASER for higher order modulation schemes. In all these studies, the CSI is assumed to be perfectly known at the Rx, which is impossible to achieve in practical systems [16], [17]. In [15], a dual-hop decode-and-forward (DF) based single-relayed NLOS UVC system is considered with multiple receiver branches at the destination node only. Selection combining is employed at the destination node and ASER performance of the system is evaluated only for rectangular quadrature amplitude modulation (QAM) scheme. In [18], the authors studied a three-node dual-hop hybrid RF/NLOS UVC system assuming imperfect CSI. RF link between source and relay is considered to follow Rayleigh distribution, and the link from the relay to the destination is considered to follow lognormal distribution under the assumption of weak atmospheric turbulence. System performance is analyzed in terms of outage probability and ASER for higher-order modulation schemes. There has been several studies conducted in the past, in which researchers evaluated the impact of imperfect CSI on the performance of RF cooperative communication systems [19]–[21]. In [19], authors evaluated the performance of a dual-hop variable-gain AF relayed RF communication system for Nakagami-m fading channel and studied the impact of imperfect CSI on the ASER performance of the system for a variety of higher order QAM schemes. In [20], a multi-relay RF communication system with best relay selection is considered with imperfect CSI at the Rx. The ASER performance of the system is analyzed for higher order modulation schemes including rectangular-QAM (RQAM), hexagonal-QAM (HQAM), and cross-QAM (XQAM) over Nakagami-m fading links. In [21], the performance of a multiple-input and multiple-output (MIMO) non-regenerative RF cooperative network with transmit antenna selection (TAS) and maximal-ratio-combining (MRC) employed at transmitter (Tx) and Rx, respectively, is studied. The authors analyzed the impact of imperfect CSI on the ASER performance of the considered system. However, since UVC channel is very different to RF, there is very limited existing research on analysis of imperfections on UVC systems. For the first time in [22], the authors considered a simplistic dual-hop AF relayed NLOS UVC system and evaluated its outage probability, and ASER for higher order modulation schemes. However, the authors in [22] did not consider the DF multi-relay case and other factors. To the best of authors knowledge, there is no other

work in the literature, which studies the impact of imperfect CSI on the performance of DF multi-relay NLOS UVC systems.

On-off keying (OOK) using intensity modulation and direct detection (IM/DD) is adopted as a popular modulation technique in OWC systems due to its simplicity [23]. However, the OOK modulation scheme is highly spectrally inefficient and is not suitable for data intensive applications [12], [24]. Further, in the case of atmospheric turbulence, OOK IM/DD requires an adaptive threshold, resulting in the increased complexity at the Rx [25]. SIM with direct detection has been proposed as an attractive alternative to OOK IM/DD in OWC systems experiencing turbulence [13], [24], [26]. In the SIM system, RF signal is pre-modulated by a data source, which is then used to modulate intensity of a continuous wave (CW) laser beam. A significant advantage offered by SIM is that it supports the use of spectrally efficient, higher-order modulation schemes such as QAM and its variants [26] including RQAM, Square-QAM (SQAM), XQAM, and HQAM [27]. SQAM is a popular and widely used modulation scheme, however, it supports only square constellations with even bits per symbol [28]. RQAM, on the other hand, is more versatile and inherently includes SQAM, M-ary amplitude shift keying (ASK), quadrature phase shift keying (QPSK), and orthogonal frequency binary shift keying (OFBSK) as special cases [29]. For odd bits per symbol, XQAM is a preferable modulation scheme as compared to RQAM due to its relatively low average and peak power requirements [30].

HQAM is an optimum two-dimensional (2D) modulation scheme, and is shown to provide significant performance gains over SQAM, RQAM, and XQAM schemes, due to the densest packing of the constellation points in 2D plane [31]. The need for bandwidth efficient modulation schemes, such as HQAM, is very much desired in NLOS UVC to support bandwidth intensive applications. This is mainly due to low-modulation speed of UV transmitters [32], which in-turn limits the achievable data rate of UVC systems in spite of huge spectrum availability in the UV band. In addition, most communication receivers estimate CSI at the Rx for symbol detection. Thus, for future applicability of UVC operating on futuristic higher-order modulation schemes, it is important to consider the impact of channel estimation errors (CEEs). To the best of authors' knowledge, the ASER analysis of higher-order modulation schemes for DF based multiple-relayed cooperative NLOS UVC system considering imperfect CSI is not studied in the literature. Main contributions of this paper are as follows:

1) For the first time in multi-relay NLOS UVC studies, we consider the practical case of imperfect CSI at the Rx and evaluate its impact on the performance of the considered multi-relay system.
2) We present a DF based cooperative NLOS UVC system employing relay selection and analyze its performance in terms of outage probability. Further, we derive the novel probability density function (PDF) expression of end-to-end (e2e) SNR of the considered system. Furthermore, we evaluate the ASER analysis for higher-order modulation schemes, such as RQAM, HQAM and XQAM, by deriving the closed-form expressions using PDF based approach.
3) We perform diversity analysis of the system and compute novel expressions of the relative diversity order (RDO) and asymptotic RDO (ARDO). The reason for computing RDO is due to the non-convergent nature of the conventional diversity order for lognormal (LN) faded UVC channels. To overcome this difficulty, the RDO is computed as an alternative performance metric in the literature. We derive the RDO and ARDO expressions by considering non-relay NLOS UVC link as the benchmark scheme and provide comprehensive analysis. We demonstrate the impact of varying number of relays and system configurations on the achieved diversity gains.
4) Although there has been considerable research in RF cooperative communication systems. However, the underlying analysis, analytical results, and inferences are not applicable to NLOS UVC system due to its entirely different channel characteristics and system configurations. The system limiting factors such as turbulence severity, elevation angles, and Rx field-of-view (FOV) are not considered in RF and VLC communication systems. Therefore, the results presented in this study are novel and useful to gain insights about multi-relay NLOS UVC performance and its dependence on various configuration parameters.

Rest of the paper is organized as follows: In Section II and Section III, the NLOS UVC channel model and the considered system models are presented, respectively. In Section IV, we derive the outage probability and PDF of the instantaneous SNR of the considered system. In Section V, the diversity analysis and derivation of the RDO and ARDO expressions are provided. In Section VI, we conduct ASER analysis for various higher-order modulation schemes. In Section VII, we present the numerical and simulation results. We finally conclude the paper in Section VIII.

II. CHANNEL MODEL

Fig. 1 shows a basic NLOS UVC channel with A and B representing the Tx and Rx, respectively. Nodes A and B are considered to be d_{AB} distance apart. θ_{AB}^{Tx} and θ_{AB}^{Rx} denote the elevation angles of A and B, respectively. ϕ_{AB}^{Tx} denotes the beam divergence of A, and ϕ_{AB}^{Rx} denotes the field-of-view (FOV) of B. The total path loss of the AB link is given as $\ell_{AB} = \ell_{AB}^{T}\ell_{AB}^{S}$ [8], where ℓ_{AB}^{S} is the path loss due to

Notations: $\mathbb{E}(\cdot)$ represents the statistical expectation operator. $Q(x) = \frac{1}{\sqrt{2\pi}}\int_x^\infty e^{-y^2/2}dy$. $\mathcal{N}(\mu, \sigma^2)$ denotes a Gaussian random variable (RV) with mean μ and variance σ^2. $f_Z(z)$ and $F_Z(z)$ represents the PDF and cumulative distribution function (CDF) of a RV Z, respectively. $\ln(\cdot)$ denotes the natural logarithm, and $\mathbb{P}[\cdot]$ represents the probability.

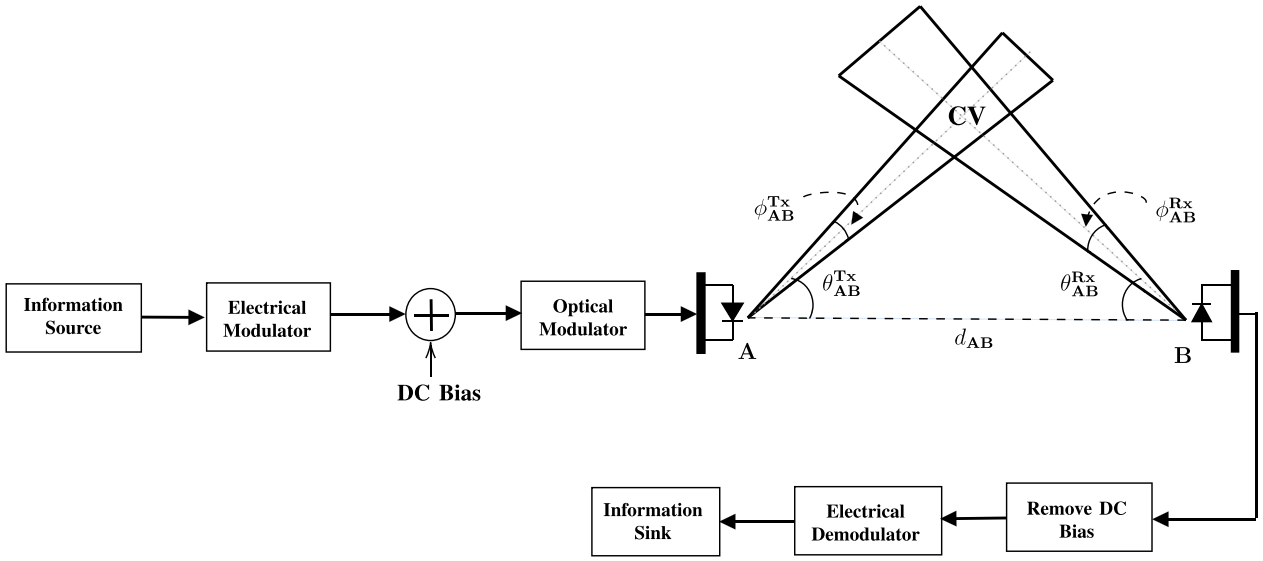

FIGURE 1. A single-input-single-output NLOS UVC link.

scattering [33] given as

$$\ell_{AB}^{S} = \frac{k_s A_r \phi_{AB}^{Tx\,2} \phi_{AB}^{Rx} \Psi(\psi) \sin\left(\theta_{AB}^{S}\right)}{96 d_{AB} \sin\left(\theta_{AB}^{Tx}\right) \sin^2\left(\theta_{AB}^{Rx}\right)\left(1-\cos\left(\phi_{AB}^{Tx}/2\right)\right)} \times \frac{\left[12\sin^2\left(\theta_{AB}^{Rx}\right) + \phi_{AB}^{Rx\,2}\sin^2\left(\theta_{AB}^{Tx}\right)\right]}{\exp\left(k_e d_{AB}\left[\sin\left(\theta_{AB}^{Tx}\right)+\sin\left(\theta_{AB}^{Rx}\right)\right]/\sin\left(\theta_{AB}^{S}\right)\right)} \quad (1)$$

and ℓ_{AB}^{T} represents the path loss due to turbulence [34] given as

$$\ell_{AB}^{T} = 10^{-0.2\sqrt{23.17 C_n^2 (2\pi/\lambda)^{7/6}}\left(\sqrt{\left(d_{AB}^{Tx}\right)^{11/6}}+\sqrt{\left(d_{AB}^{Rx}\right)^{11/6}}\right)}. \quad (2)$$

Here, λ is wavelength of the UV wave, C_n^2 represents the refractive index structure parameter of the atmosphere, and $\theta_{AB}^{S} = \theta_{AB}^{Tx} + \theta_{AB}^{Rx}$ is the scattering angle. d_A^{Tx} and d_B^{Rx} are the distances from Tx and Rx to the common volume (CV), respectively. k_s is the scattering coefficient which is computed as the sum of Rayleigh scattering coefficient k_s^{Ray} and Mie scattering coefficient k_s^{Mie}. The extinction coefficient, $k_e = k_s + k_a$ with k_a as the absorption coefficient of the atmosphere. $\Psi(\cdot)$ is the scattering phase function computed as

$$\Psi(\psi) = \frac{1}{k_s}\left[k_s^{Ray}\Psi^{Ray}(\psi) + k_s^{Mie}\Psi^{Mie}(\psi)\right], \quad (3)$$

where $\psi = \cos(\theta_{AB}^{S})$. $\Psi^{Ray}(\cdot)$ is the Rayleigh scattering phase function given by

$$\Psi^{Ray}(\psi) = \frac{3\left[1+3\gamma+(1-\gamma)\psi^2\right]}{16\pi(1+2\gamma)}, \quad (4)$$

and $\Psi^{Mie}(\cdot)$ is the Mie scattering phase function defined as

$$\Psi^{Mie}(\psi) = \left(\frac{1-r^2}{4\pi}\right) \times \left[\frac{1}{\left(1+r^2-2r\psi\right)^{3/2}} + f\frac{0.5\left(3\psi^2-1\right)}{\left(1+r^2\right)^{3/2}}\right], \quad (5)$$

where γ is the parameter of Rayleigh scattering phase function. The value of this parameter is defined as 0.017 for $\lambda = 260$ nm, terrestrial atmosphere and standard air [8], [33], [35]. r and f are the parameters of Mie scattering phase function with values 0.72 and 0.5, respectively, [33]. These values result in an excellent fit to the UV phase functions computed from Mie theory for a particular power-law aerosol size distribution [8], [33], [36].

Atmospheric turbulence arises due to the change in temperature and air pressure with distance, resulting in inhomogeneous environmental conditions and variations in the atmospheric refractive index. This atmospheric turbulence manifests itself as fluctuations in the received optical irradiance, referred to as turbulence-induced fading. Scintillation index ($\sigma_{h_{AB}}^2$) is used to quantify the turbulence strength. For plane wave propagation, the scintillation index of a LOS link is computed using the Rytov variance as [8], [12], [34]

$$\sigma_{h_{AB}}^2 = 1.23 C_n^2 k^{7/6} d_{AB}^{11/6}, \quad (6)$$

where C_n^2 is the refractive index structure coefficient, and $k = 2\pi/\lambda$ with λ is the wavelength. For $\sigma_{h_{AB}}^2 \leq 1.2$, the turbulence is considered as weak and in such case, lognormal distribution with PDF given below is used to model the irradiance fluctuations h_{AB} [8].

$$f_{h_{AB}}(h) = \frac{1}{\sqrt{2\pi}\,\sigma_{h_{AB}} h}\exp\left(\frac{-\left(\ln(h)-\mu_{h_{AB}}\right)^2}{2\sigma_{h_{AB}}^2}\right), \quad (7)$$

where $\mu_{h_{AB}}$ and $\sigma_{h_{AB}}^2$ are the mean and variance of $\ln(h_{AB})$, respectively. With the single scattering assumption, the NLOS UVC link consists of two LOS paths, one from node A to the common volume (CV) and another from the CV to node B as shown in Fig. 1. Under weak turbulence conditions, the overall PDF of the irradiance fluctuations for AB NLOS link is lognormally distributed with scintillation index given by the sum of scintillation index of individual links [8]

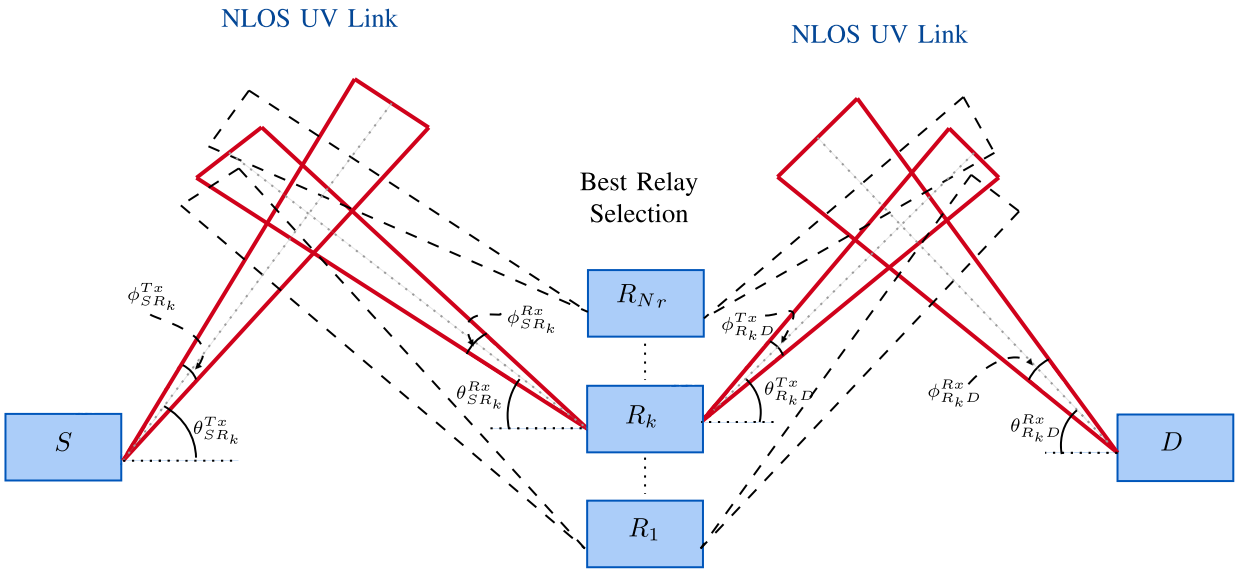

FIGURE 2. A multi-relay NLOS UVC system with best relay selection.

$\sigma^2_{h_{A,B}} = \sigma^2_{h_{A,CV}} + \sigma^2_{h_{CV,B}}$ with $\sigma^2_{h_{A,CV}} = 1.23C_n^2k^2{d^{Tx}_{AB}}^{11/6}$, and $\sigma^2_{h_{CV,B}} = 1.23C_n^2k^2{d^{Rx}_{AB}}^{11/6}$. The distance of the CV from A and B node can be computed as [8],

$$d^{Tx}_{AB} = \frac{d\sin(\theta^{Rx}_{AB})}{\sin(\theta^{Tx}_{AB}+\theta^{Rx}_{AB})}, \quad d^{Rx}_{AB} = \frac{d\sin(\theta^{Tx}_{AB})}{\sin(\theta^{Tx}_{AB}+\theta^{Rx}_{AB})}. \tag{8}$$

III. SYSTEM MODEL

In this work, we consider a dual-hop planar NLOS UVC system which has a source (S), a destination (D) and N_r parallel relays R_k, $k = 1 \ldots N_r$ as shown in Fig. 2. All the nodes are assumed to operate in half-duplex mode. The channel coefficients corresponding to SR_k and R_kD links are independent and follow LN distribution for weak turbulence case. The relays are configured with the same elevation angles and FOVs, resulting in identical distribution of h_{SR_k} links,

$$\ln(h_{SR_k}) \sim \mathcal{N}\left(\mu_{h_{SR_k}}, \sigma^2_{h_{SR_k}}\right), \tag{9}$$

with $\mu_{h_{SR_k}} = \mu_{h_{SR}}$ and $\sigma_{h_{SR_k}} = \sigma^2_{h_{SR}}$, $k = 1 \ldots N_r$; and identical distribution of h_{R_kD} links,

$$\ln(h_{R_kD}) \sim \mathcal{N}\left(\mu_{h_{R_kD}}, \sigma^2_{h_{R_kD}}\right) \tag{10}$$

with $\mu_{h_{R_kD}} = \mu_{h_{RD}}$ and $\sigma_{h_{R_kD}} = \sigma^2_{h_{RD}}$, $k = 1 \ldots N_r$. Further, with similar system configurations the path loss of SR_k and R_kD links are given as $\ell_{SR_k} = \ell_{SR}$ and $\ell_{R_kD} = \ell_{RD}$, respectively.

To avoid the adaptive threshold requirement of OOK modulation and to achieve higher spectral efficiency, we use SIM at Tx. In case of SIM, a data source is pre-modulated in the electrical domain using the desired modulation scheme. Next, an appropriate DC bias is added to move the constellation of electrically modulated signal to the first quadrant. Finally, the pre-modulated RF signal ($s(t)$) is used to modulate the intensity of a continuous ultraviolet (UV) laser beam [26]. The resultant transmitted optical signal is given as $x(t) = P[1 + \eta\iota_{eo}s(t)]$, where ι_{eo} is the the electrical to optical conversion efficiency, and P is the average transmit optical power. The modulation index η is chosen such that $-1 < \eta\iota_{eo}s(t) < 1$ to avoid over modulation [24], [26]. There are two practical issues associated with SIM [37]: (i) poor power efficiency due to the addition of DC biasing with the pre-modulated RF subcarrier signal. The power efficiency becomes worse for multiple-SIM (MSM), in which multiple subcarriers are used, (ii) requirement of accurate synchronization of carrier phases when complex modulation schemes are adopted.

The poor power efficiency of SIM in our case is limited due to the consideration of a single SIM. We have also adopted the highly spectrally efficient modulation schemes that provide significant SNR gain for a target ASER, thereby compensating for the poor power efficiency of SIM. In SIM systems, the receiver employs a phase-locked loop (PLL) to track the phase of the electrical signal received at the output of the photo-detector. Error in the phase tracking results in poor system performance. Extensive research studies carried out in the literature to study the effect of carrier phase recovery error (CPE) on the system performance [38]. In the current work, we have assumed that the carrier phase is perfectly synchronized.

At the UVC Rx, in practice, the CSI is not known a priori, and is thus estimated prior to the symbol detection. Considering minimum mean square error estimation (MMSE) at the Rx, the actual channel (h_m) and its estimate ($\hat{h}_m$) are related as $h_m = \hat{h}_m + e_m$, where $e_m \sim \mathcal{N}(0, \sigma^2_{e,m})$ is the CEE with $\sigma^2_{e,m} = \frac{v_{h_m}}{1+\rho\ell^2_m\chi_\circ v_{h_m}}$, $m \in \{SR_k, R_kD\}$ [19]–[22]. $v_{h_m} = [\exp(\sigma^2_{h_m}) - 1]\exp(2\mu_{h_m} + \sigma^2_{h_m})$ is the variance of h_m,

$\rho > 0$ represents quality of the channel estimate, and $\chi_\circ$ is the average received SNR of the non-relayed link.

The instantaneous electrical SNR of the SR_kD link at Rx is given as

$$\chi_{DF}^{(k)} = \min\left(\chi_{SR_k}, \chi_{R_kD}\right), \tag{11}$$

where $\chi_m = \frac{\ell_m^2 t_{eo}^2 \iota_{oe}^2 \chi_\circ \hat{h}_m^2}{4(1+\ell_m^2 \sigma_{e,m}^2 \chi_\circ)}$, $m \in \{SR_k, R_kD\}$ represents the instantaneous SNR of the m^{th} link in which i_{eo} is the optical to electrical conversion efficiency of the photodetector (PD). For moderate to high SNRs, $\sigma_{e,m}^2$ is very small as compared to v_{h_m}, and hence, the distribution of h_m and $\hat{h}_m$ is considered as approximately same with negligible impact on the performance analysis [19], [39]. Using the properties of LN RVs, it can be shown that χ_m also follows LN distribution as

$$\ln(\chi_m) \sim \mathcal{N}\left(2\mu_{h_m} - \ln\left(4\epsilon_m + 4\sigma_{e,m}^2\right), 2\sigma_{h_m}\right), \tag{12}$$

where $\epsilon_m = \ell_m^{-2}\chi_\circ^{-1}$. We consider best-relay selection in which the relay with the highest SNR is selected for communication to D [40]. Due to relatively high path loss of SD link ($\sim$ 123 dB for 1 Km distance [33]) as compared to SR_kD link, the SNR of the SD link is not considered by the selection combiner at D for UVC cases. Thus, the instantaneous e2e electrical SNR at node D is given by

$$\chi_{e2e} = \max_{k=1\ldots N_r} \chi_{DF}^{(k)}. \tag{13}$$

In the next Section, we will use the e2e SNR (χ_{e2e}) to compute outage probability of the considered system.

IV. OUTAGE PROBABILITY

Outage probability is defined as the probability of instantaneous SNR of the system falling below a predefined threshold, χ_{th}. From (11) the outage probability of SR_kD link is given as

$$P_{out}^{SR_kD} = \mathbb{P}\left[\chi_{DF}^{(k)} \le \chi_{th}\right] = F_{\chi_{DF}^{(k)}}(\chi_{th}), \tag{14}$$

where $F_{\chi_{DF}^{(k)}}(\chi_{th})$ is recognized as the CDF of $\chi_{DF}^{(k)}$. On substituting (11) into (14) and rearranging, we get

$$F_{\chi_{DF}^{(k)}} = 1 - \mathbb{P}\left[\min\left(\chi_{SR_k}, \chi_{R_kD}\right) \ge \chi_{th}\right]. \tag{15}$$

For independent RVs χ_{SR_k} and χ_{R_kD}, (15) can alternatively be represented as [8]

$$F_{\chi_{DF}^{(k)}} = 1 - \left[1 - F_{\chi_{SR_k}}(\chi_{th})\right]\left[1 - F_{\chi_{SR_k}}(\chi_{th})\right], \tag{16}$$

where $F_{\chi_{SR_k}}(\cdot)$ and $F_{\chi_{R_kD}}(\cdot)$ represent CDFs of RVs χ_{SR_k} and χ_{R_kD}, respectively. For independent RVs $\chi_{DF}^{(1)}, \chi_{DF}^{(2)}, \ldots \chi_{DF}^{(N_r)}$, the outage probability of the e2e system can be computed from (13) and (16) as [41]

$$P_{out}^{e2e} = \prod_{k=1}^{N_r}\left(1 - \left[1 - F_{\chi_{SR_k}}(\chi_{th})\right]\left[1 - F_{\chi_{R_kD}}(\chi_{th})\right]\right). \tag{17}$$

On substituting the CDFs of identically distributed LN RVs $\{\chi_{SR_k}\}_{k=1}^{N_r}$ and $\{\chi_{R_kD}\}_{k=1}^{N_r}$ into (17), we get the following closed expression of the outage probability for the considered system.[1]

$$P_{out}^{e2e} = \left[1 - Q\left(\frac{\ln(\chi) - 2\mu_{h_{SR}} + \ln\left(4\epsilon_{SR} + 4\sigma_{e,SR}^2\right)}{2\sigma_{h_{SR}}}\right) \times Q\left(\frac{\ln(\chi) - 2\mu_{h_{RD}} + \ln\left(4\epsilon_{RD} + 4\sigma_{e,RD}^2\right)}{2\sigma_{h_{RD}}}\right)\right]^{N_r}. \tag{18}$$

Note that, for notational simplicity, we have replaced the symbol χ_{th} with χ in (18). Further, observing P_{out}^{e2e} as the CDF of χ_{e2e}, we differentiate (18) with respect to χ to obtain the PDF for χ_{e2e} as

$$\begin{aligned} f_{\chi_{e2e}}(\chi) &= N_r\left[f_{\chi_{SR}}(\chi)Q\left(\frac{\ln(\chi) - 2\mu_{h_{RD}} + \ln\left(4\epsilon_{RD} + 4\sigma_{e,RD}^2\right)}{2\sigma_{h_{RD}}}\right) + f_{\chi_{RD}}(\chi)Q\left(\frac{\ln(\chi) - 2\mu_{h_{SR}} + \ln\left(4\epsilon_{SR} + 4\sigma_{e,SR}^2\right)}{2\sigma_{h_{SR}}}\right)\right] \\ &\times \left[1 - Q\left(\frac{\ln(\chi) - 2\mu_{h_{SR}} + \ln\left(4\epsilon_{SR} + 4\sigma_{e,SR}^2\right)}{2\sigma_{h_{SR}}}\right) \times Q\left(\frac{\ln(\chi) - 2\mu_{h_{RD}} + \ln\left(4\epsilon_{RD} + 4\sigma_{e,RD}^2\right)}{2\sigma_{h_{RD}}}\right)\right]^{N_r-1}, \end{aligned} \tag{19}$$

where $f_{\chi_j}(\chi) = \frac{1}{\sqrt{2\pi}\,2\sigma_{h_j}} \exp\left[\frac{-(\ln(\chi) - 2\mu_{h_j} + \ln(4\epsilon_j + 4\sigma_{e,j}^2))^2}{8\sigma_{h_j}^2}\right]$, $j \in \{SR, RD\}$. The $f_{\chi_{e2e}}(\chi)$ is used in deriving analytical expressions of ASER in later sections. Therefore, we define Theorem 1 which compute ensemble average of an arbitrary function of χ_{e2e} using the PDF derived in (19).

Theorem 1: Let $g(\cdot)$ be an arbitrary function of RV χ_{e2e}, whose PDF is given in (19). The ensemble average of $g(\chi_{e2e})$ can be computed as

$$\begin{aligned} \mathbb{E}\left[g(\chi_{e2e})\right] &= \int_0^\infty g(\chi) f_{\chi_{e2e}}(\chi) d\chi = \frac{N_r}{\sqrt{\pi}} \sum_{n=1}^{N} w_n \\ &\times g\left(\exp\left(\kappa_n^{SR} - \ln\left(4\epsilon_{SR} + 4\sigma_{e,SR}^2\right)\right)\right) \\ &\times Q\left(\Delta_{RD}\kappa_n^{SR} - \Upsilon_{RD} - \Delta_{RD}\ln(\vartheta)\right) \\ &\times \left[\left(1 - Q\left(\sqrt{2}\xi_n\right)\right) \times Q\left(\Delta_{RD}\kappa_n^{SR} - \Upsilon_{RD} - \Delta_{RD}\ln(\vartheta)\right)\right]^{N_r-1} \\ &+ \frac{N_r}{\sqrt{\pi}} \sum_{n=1}^{N} w_n g\left(\exp\left(\kappa_n^{RD} - \ln\left(4\epsilon_{RD} + 4\sigma_{e,RD}^2\right)\right)\right) \end{aligned}$$

1. Using (9) and (10), $\sigma_{e,SR} = \sigma_{e,SR_k}, \epsilon_{SR} = \epsilon_{SR_k}, \sigma_{e,RD} = \sigma_{e,R_kD}$, and $\epsilon_{RD} = \epsilon_{R_kD}$ for $k = 1 \ldots N_r$.

$$\times Q\Big(\Delta_{SR}\kappa_n^{RD} - \Upsilon_{SR} + \Delta_{SR}\ln(\vartheta)\Big) \times \Big[1 - Q\Big(\sqrt{2}\xi_n\Big)Q\Big(\Delta_{SR}\kappa_n^{RD} - \Upsilon_{SR} + \Delta_{SR}\ln(\vartheta)\Big)\Big]^{N_r-1}, \tag{20}$$

where $\kappa_n^j = 2\sqrt{2}\,\sigma_{h_j}\xi_n + 2\mu_{h_j}$, $\Delta_j = 1/2\sigma_{h_j}$, $\Upsilon_j = \mu_{h_j}/\sigma_{h_j}$ with $j \in \{SR, RD\}$, and $\vartheta = (\epsilon_{SR} + \sigma_{e,SR}^2)/(\epsilon_{RD} + \sigma_{e,RD}^2)$. w_n and ξ_n are the weights and zeros of N^{th} order Hermite polynomial, respectively.

Proof: See Appendix A. ■

V. DIVERSITY ANALYSIS

A. RELATIVE DIVERSITY ORDER (RDO)

Diversity order is an important metric to evaluate comparative performance of multi-relay wireless communication systems for different number of relays [8], [13], [19]. The conventional diversity order of a lognormally distributed fading channel does not converge to a finite value. In such case, RDO is computed as a useful measure to quantify the diversity advantage of a system as compared to some benchmark scheme. RDO was first introduced in [42] and thereafter widely adopted in the cooperative communication literature involving LN fading channels [8], [43], [44]. For systems incorporating multiple relays, non-relayed (*SD* link) is typically considered as the benchmark scheme [8]. With this consideration, the RDO of the system is defined as,

$$\text{RDO} = \frac{\partial \ln P_{out}^{e2e}/\partial \ln \chi_\circ}{\partial \ln P_{out}^{SD}/\partial \ln \chi_\circ}, \tag{21}$$

where

$$P_{out}^{SD} = 1 - Q\left(\frac{\ln(\chi) - 2\mu_{h_{SD}} + \ln\Big(4\epsilon_{SD} + 4\sigma_{e,SD}^2\Big)}{2\sigma_{h_{SD}}}\right) \tag{22}$$

is the outage probability of the *SD* link.

Theorem 2: The RDO of the considered system is computed as

$$\begin{aligned}\text{RDO} &= \frac{2\sigma_{h_{SD}}N_r Q\Big(\frac{\ln(\chi_\circ)-\ln(\zeta_{SD})+2\mu_{h_{SD}}}{2\sigma_{h_{SD}}}\Big)}{\exp\Big(\frac{-\big(\ln(\chi_\circ)-\ln(\zeta_{SD})+2\mu_{h_{SD}}\big)^2}{8\sigma_{h_{SD}}^2}\Big)} \\ &\times\Bigg[\frac{\frac{1}{2\sigma_{h_{SR}}}\exp\Big(\frac{-\big(\ln(\chi_\circ)-\ln(\zeta_{SR})+2\mu_{h_{SR}}\big)^2}{8\sigma_{h_{SR}}^2}\Big)}{Q\Big(\frac{\ln(\chi_\circ)-\ln(\zeta_{SR})+2\mu_{h_{SR}}}{2\sigma_{h_{SR}}}\Big)+Q\Big(\frac{\ln(\chi_\circ)-\ln(\zeta_{RD})+2\mu_{h_{RD}}}{2\sigma_{h_{RD}}}\Big)} \\ &+\frac{\frac{1}{2\sigma_{h_{RD}}}\exp\Big(\frac{-\big(\ln(\chi_\circ)-\ln(\zeta_{RD})+2\mu_{h_{RD}}\big)^2}{8\sigma_{h_{RD}}^2}\Big)}{Q\Big(\frac{\ln(\chi_\circ)-\ln(\zeta_{SR})+2\mu_{h_{SR}}}{2\sigma_{h_{SR}}}\Big)+Q\Big(\frac{\ln(\chi_\circ)-\ln(\zeta_{RD})+2\mu_{h_{RD}}}{2\sigma_{h_{RD}}}\Big)}\Bigg],\end{aligned} \tag{23}$$

where $\zeta_p = 4\ell_p^{-2}\chi^{-1}, p \in \{SD, SR, RD\}$ with χ is the threshold SNR.

Proof: See Appendix B. ■

The RDO expression of (23) is quite complex and does not explicitly state about the obtained diversity order and its dependence on the system configuration. To gain further insights on the achieved diversity gain, we compute the asymptotic value of the RDO at high SNR values below.

B. ASYMPTOTIC RDO (ARDO)

The ARDO is computed as higher SNR approximation of RDO as [42]

$$\text{ARDO} = \lim_{\chi_\circ \to \infty} \text{RDO}. \tag{24}$$

Theorem 3: The ARDO of considered system is given as

$$\text{ARDO} \approx N_r\sigma_{h_{SD}}^2\left[\Big(\sigma_{h_{SR}}^{-1} - \sigma_{h_{RD}}^{-1}\Big)^2 + \sigma_{h_{SR}}^{-1}\sigma_{h_{RD}}^{-1}\right]. \tag{25}$$

Proof: See Appendix C. ■

Corollary 1: For the special case of same elevation angles at S, R, and D; and $d_{SR} = d_{RD} = d_{SD}/2$, the ARDO expression converges to $N_r 2^{11/6}$. ■

It is noteworthy to see that, due to its simplicity, ARDO gives more insight about the achieved diversity order as compared to RDO derived in the previous section. ARDO expression clearly shows dependence of the diversity order on the number of relays, and scintillation indexes of SR_k, R_kD and SD links. It can be inferred that for a fixed $\sigma_{h_{SD}}^2$, relative diversity order of the system is directly proportional to N_r, however, the presence of additional term $(\sigma_{h_{SR}}^{-1} - \sigma_{h_{RD}}^{-1})^2 + \sigma_{h_{SR}}^{-1}\sigma_{h_{RD}}^{-1}$ lowers the diversity order of system for high turbulence scenarios. The same is expected because due to high turbulence, the optical wave front distortion becomes more prominent, thereby resulting in increased molecular dispersion, and deteriorated system performance [45]. Further, from Corollary 1, it can be observed that the dependence of the diversity order on scintillation index vanishes when identical configurations are chosen for SR_k, R_kD and SD links.

VI. ASER ANALYSIS

In this Section, we present the ASER analysis of the considered system for a variety of different modulation schemes including *RQAM*, *HQAM* and *XQAM* − 32. Using the PDF based approach, the ASER expression of the system can be computed as [12]

$$P_s(e) = \int_0^\infty P_s(e|\chi) f_{\chi_{e2e}}(\chi) d\chi, \tag{26}$$

where $P_s(e|\chi)$ is the conditional symbol error rate (SER) for the AWGN channel, and $f_{\chi_{e2e}}(\chi)$ is the PDF of the e2e SNR of the system given by (19).

A. RECTANGULAR QAM SCHEME

The conditional SER expression of RQAM-$M_I \times M_Q$ scheme is given as

$$P_s^{\text{RQAM}}(e|\chi) = 2pQ\big(A\sqrt{\chi}\big) + 2qQ\big(B\sqrt{\chi}\big) - 4pqQ\big(A\sqrt{\chi}\big)Q\big(B\sqrt{\chi}\big), \tag{27}$$

where $A = \sqrt{6/((M_I^2-1)(M_Q^2-1)\beta^2)}$, $B = \beta A$, $p = 1 - 1/M_I$, $q = 1 - 1/M_Q$. β is the ratio of quadrature and in-phase distances represented as d_Q and d_I, respectively. On substituting the (27) into (26) and applying Theorem 1, we obtain the ASER expression of the RQAM scheme as

$$
\begin{aligned}
&P_s^{\text{RQAM}} \\
&= \frac{N_r}{\sqrt{\pi}} \sum_{n=1}^{N} w_n \Bigg[2pQ\Bigg(A\sqrt{\exp\Big(\kappa_n^{SR} - \ln\Big(4\epsilon_{SR} + 4\sigma_{e,SR}^2\Big)\Big)}\Bigg) \\
&\qquad + 2qQ\Bigg(B\sqrt{\exp\Big(\kappa_n^{SR} - \ln\Big(4\epsilon_{SR} + 4\sigma_{e,SR}^2\Big)\Big)}\Bigg) \\
&\qquad - 4pqQ\Bigg(A\sqrt{\exp\Big(\kappa_n^{SR} - \ln\Big(4\epsilon_{SR} + 4\sigma_{e,SR}^2\Big)\Big)}\Bigg) \\
&\qquad \times Q\Bigg(B\sqrt{\exp\Big(\kappa_n^{SR} - \ln\Big(4\epsilon_{SR} + 4\sigma_{e,SR}^2\Big)\Big)}\Bigg)\Bigg] \\
&\quad \times Q\Big(\Delta_{RD}\kappa_n^{SR} - \Upsilon_{RD} - \Delta_{RD}\ln(\vartheta)\Big) \\
&\quad \times \Big[1 - Q\Big(\sqrt{2}\xi_n\Big)Q\Big(\Delta_{RD}\kappa_n^{SR} - \Upsilon_{RD} - \Delta_{RD}\ln(\vartheta)\Big)\Big]^{N_r-1} \\
&\quad + \frac{N_r}{\sqrt{\pi}} \sum_{n=1}^{N} w_n \Bigg[2pQ\Bigg(A\sqrt{\exp\Big(\kappa_n^{RD} - \ln\Big(4\epsilon_{RD} + 4\sigma_{e,RD}^2\Big)\Big)}\Bigg) \\
&\qquad + 2qQ\Bigg(B\sqrt{\exp\Big(\kappa_n^{RD} - \ln\Big(4\epsilon_{RD} + 4\sigma_{e,RD}^2\Big)\Big)}\Bigg) \\
&\qquad - 4pqQ\Bigg(A\sqrt{\exp\Big(\kappa_n^{RD} - \ln\Big(4\epsilon_{RD} + 4\sigma_{e,RD}^2\Big)\Big)}\Bigg) \\
&\qquad \times Q\Bigg(B\sqrt{\exp\Big(\kappa_n^{RD} - \ln\Big(4\epsilon_{RD} + 4\sigma_{e,RD}^2\Big)\Big)}\Bigg)\Bigg] \\
&\quad \times Q\Big(\Delta_{SR}\kappa_n^{RD} - \Upsilon_{SR} + \Delta_{SR}\ln(\vartheta)\Big) \\
&\quad \times \Big[1 - Q\Big(\sqrt{2}\xi_n\Big)Q\Big(\Delta_{SR}\kappa_n^{RD} - \Upsilon_{SR} + \Delta_{SR}\ln(\vartheta)\Big)\Big]^{N_r-1}.
\end{aligned}
\tag{28}
$$

Additionally, the expression for M-ary SQAM scheme can directly be obtained from (28) by substituting $M = \sqrt{M_I} = \sqrt{M_Q}$ [21].

B. HEXAGONAL QAM SCHEME

The condition SER expression of M-ary HQAM constellation for AWGN channel is given as

$$
\begin{aligned}
P_s^{\text{HQAM}}(e|\chi) = DQ\big(\sqrt{q\chi}\big) + \frac{2}{3}D_C Q^2\Big(\sqrt{2q\chi/3}\Big) \\
- 2D_C Q\big(\sqrt{q\chi}\big)Q\Big(\sqrt{q\chi/3}\Big),
\end{aligned}
\tag{29}
$$

where q, D, and D_C are the constants which are defined in [12] for different constellation sizes. Substituting (29) into (26), and applying Theorem 1 results in the following ASER expression of M-ary HQAM scheme for the considered system.

$$
\begin{aligned}
&P_s^{\text{HQAM}} \\
&= \frac{N_r}{\sqrt{\pi}} \sum_{n=1}^{N} w_n \\
&\quad \times \Bigg[DQ\Bigg(\sqrt{q\exp\Big(\kappa_n^{SR} - \ln\Big(4\epsilon_{SR} + 4\sigma_{e,SR}^2\Big)\Big)}\Bigg) \\
&\qquad + \frac{2}{3}D_C Q^2\Bigg(\sqrt{\frac{2q}{3}\exp\Big(\kappa_n^{SR} - \ln\Big(4\epsilon_{SR} + 4\sigma_{e,SR}^2\Big)\Big)}\Bigg) \\
&\qquad - 2D_C Q\Bigg(\sqrt{q\exp\Big(\kappa_n^{SR} - \ln\Big(4\epsilon_{SR} + 4\sigma_{e,SR}^2\Big)\Big)}\Bigg) \\
&\qquad \times Q\Bigg(\sqrt{\frac{q}{3}\exp\Big(\kappa_n^{SR} - \ln\Big(4\epsilon_{SR} + 4\sigma_{e,SR}^2\Big)\Big)}\Bigg)\Bigg] \\
&\quad \times Q\Big(\Delta_{RD}\kappa_n^{SR} - \Upsilon_{RD} - \Delta_{RD}\ln(\vartheta)\Big) \\
&\quad \times \Big[1 - Q\Big(\sqrt{2}\xi_n\Big)Q\Big(\Delta_{RD}\kappa_n^{SR} - \Upsilon_{RD} - \Delta_{RD}\ln(\vartheta)\Big)\Big]^{N_r-1} \\
&\quad + \frac{N_r}{\sqrt{\pi}} \sum_{n=1}^{N} w_n \Bigg[DQ\Bigg(\sqrt{q\exp\Big(\kappa_n^{RD} - \ln\Big(4\epsilon_{RD} + 4\sigma_{e,RD}^2\Big)\Big)}\Bigg) \\
&\qquad + \frac{2}{3}D_C Q^2\Bigg(\sqrt{\frac{2q}{3}\exp\Big(\kappa_n^{RD} - \ln\Big(4\epsilon_{RD} + 4\sigma_{e,RD}^2\Big)\Big)}\Bigg) \\
&\qquad - 2D_C Q\Bigg(\sqrt{q\exp\Big(\kappa_n^{RD} - \ln\Big(4\epsilon_{RD} + 4\sigma_{e,RD}^2\Big)\Big)}\Bigg) \\
&\qquad \times Q\Bigg(\sqrt{\frac{q}{3}\exp\Big(\kappa_n^{RD} - \ln\Big(4\epsilon_{RD} + 4\sigma_{e,RD}^2\Big)\Big)}\Bigg)\Bigg] \\
&\quad \times Q\Big(\Delta_{SR}\kappa_n^{RD} - \Upsilon_{SR} + \Delta_{SR}\ln(\vartheta)\Big) \\
&\quad \times \Big[1 - Q\Big(\sqrt{2}\xi_n\Big)Q\Big(\Delta_{SR}\kappa_n^{RD} - \Upsilon_{SR} + \Delta_{SR}\ln(\vartheta)\Big)\Big]^{N_r-1}.
\end{aligned}
\tag{30}
$$

C. CROSS QAM SCHEME

Here, we derive the ASER expression of XQAM scheme for constellation size of 32 (XQAM-32). The conditional SER expression of XQAM for AWGN channel is given as [30]

$$
\begin{aligned}
P_s^{\text{XQAM-32}}(e|\chi) = \frac{1}{8}\Big[26Q\Big(\sqrt{2C\chi}\Big) + Q\Big(2\sqrt{C\chi}\Big) \\
- 23Q^2\Big(\sqrt{2C\chi}\Big)\Big],
\end{aligned}
\tag{31}
$$

where $C = \frac{48}{31M-32}$. Here, M is the constellation size of M-ary XQAM scheme. For XQAM-32, $M = 32$ which results in $C = 0.05$. Using (31) into (26) and applying Theorem 1, we obtain the ASER expression of XQAM-32 scheme as

$$
\begin{aligned}
&P_s^{\text{XQAM-32}} \\
&= \frac{N_r}{8\sqrt{\pi}} \sum_{n=1}^{N} w_n \\
&\quad \times \Bigg[26Q\Bigg(\sqrt{2C\exp\Big(\kappa_n^{SR} - \ln\Big(4\epsilon_{SR} + 4\sigma_{e,SR}^2\Big)\Big)}\Bigg) \\
&\qquad + Q\Bigg(2\sqrt{C\exp\Big(\kappa_n^{SR} - \ln\Big(4\epsilon_{SR} + 4\sigma_{e,SR}^2\Big)\Big)}\Bigg) \\
&\qquad - 23Q^2\Bigg(\sqrt{2C\exp\Big(\kappa_n^{SR} - \ln\Big(4\epsilon_{SR} + 4\sigma_{e,SR}^2\Big)\Big)}\Bigg)\Bigg] \\
&\quad \times Q\Big(\Delta_{RD}\kappa_n^{SR} - \Upsilon_{RD} - \Delta_{RD}\ln(\vartheta)\Big) \\
&\quad \times \Big[1 - Q\Big(\sqrt{2}\xi_n\Big)Q\Big(\Delta_{RD}\kappa_n^{SR} - \Upsilon_{RD} - \Delta_{RD}\ln(\vartheta)\Big)\Big]^{N_r-1}
\end{aligned}
$$

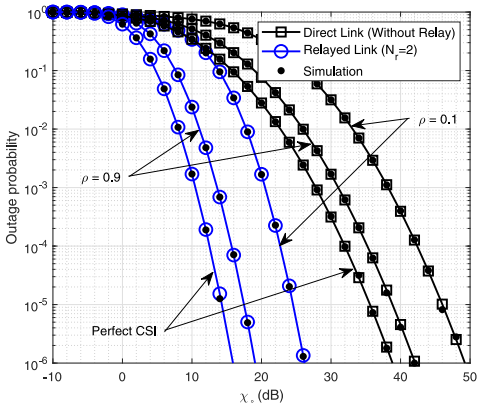

(a) Comparison of analytical and simulation results of P_{out} versus $\chi_\circ$ with the benchmark system for $N_r = 2$.

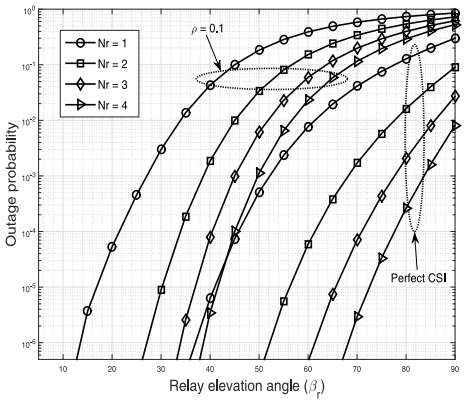

(b) P_{out} versus relay elevation angle (β_r) for $N_r = (1, 2, 3, 4)$ and $\psi_\circ = 10$ dB.

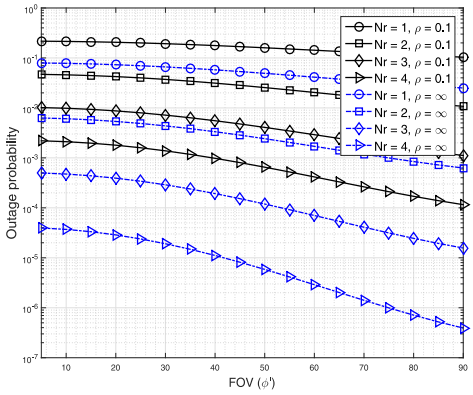

(c) P_{out} versus FOV (ϕ') for $\rho = (0.1, \infty)$ and $\psi_\circ = 10$ dB.

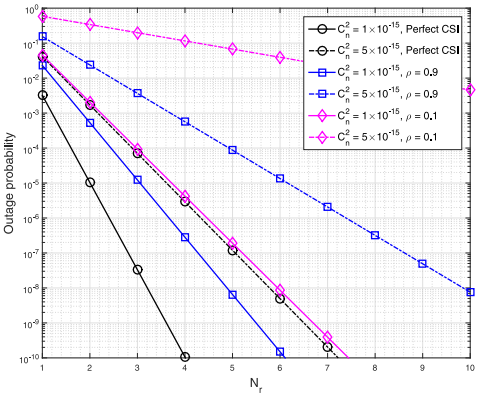

(d) P_{out} versus N_r for different turbulence strength (C_n^2), $\rho = (0.1, 0.9, \infty)$ and $\psi_\circ = 10$ dB.

FIGURE 3. Outage probability results for different average SNRs, number of relays, elevation angles, Rx FOVs, and turbulence strength (C_n^2).

$$+\frac{N_r}{\sqrt{8\pi}}\sum_{n=1}^{N} w_n \times \left[26Q\left(\sqrt{2C\exp\left(\kappa_n^{RD} - \ln\left(4\epsilon_{RD} + 4\sigma_{e,RD}^2\right)\right)}\right) + Q\left(2\sqrt{C\exp\left(\kappa_n^{RD} - \ln\left(4\epsilon_{RD} + 4\sigma_{e,RD}^2\right)\right)}\right) - 23Q^2\left(\sqrt{2C\exp\left(\kappa_n^{RD} - \ln\left(4\epsilon_{RD} + 4\sigma_{e,RD}^2\right)\right)}\right)\right] \times Q\left(\Delta_{SR}\kappa_n^{RD} - \Upsilon_{SR} + \Delta_{SR}\ln(\vartheta)\right)\left[1 - Q\left(\sqrt{2}\xi_n\right) \times Q\left(\Delta_{SR}\kappa_n^{RD} - \Upsilon_{SR} + \Delta_{SR}\ln(\vartheta)\right)\right]^{N_r-1}. \quad (32)$$

VII. NUMERICAL AND SIMULATION RESULTS

In this Section, we present numerical investigations, and validate accuracy of the derived analytical expressions using Monte-Carlo simulations. Unless otherwise stated, we consider $\lambda = 260$ nm, $k_s^{Ray} = 2.4\times10^{-4}$ m^{-1}, $k_s^{Mie} = 2.5\times10^{-4}$ m^{-1}, $k_a = 9\times10^{-4}$ m^{-1}, $C_n^2 = 5\times10^{-15}$ m$^{-2/3}$, $\iota_{eo} = \iota_{oe} = 1$, and Rx aperture area $A_r = 1.77$ cm^2. Distance between S and D nodes is $d_{SD} = 1000$ m [8], [12] and relays are assumed to be placed in the middle of S and D, $d_{SR_k} = d_{R_kD} = 500$ m. Further, elevation angles are configured as $\theta_{SR_k}^{Tx} = \theta_{R_kD}^{Rx} = 30°$, and $\theta_{SR_k}^{Rx} = \theta_{R_kD}^{Tx} = 70°$ [8]. Furthermore, the beam divergence of Tx and FOV of Rx are considered to be 10° and 60°, respectively [33].

In Fig. 3, outage probability of the considered multi-relay system are presented for different system configurations, ρ values and turbulence strengths. Fig. 3(a) compares the analytical and simulation results of the outage probability versus $\chi_\circ$ for $N_r = 2$, considering both the perfect CSI ($\rho \to \infty$) and imperfect CSI ($\rho = 0.1, 0.9$) cases. It can be observed that the simulation results overlap with the theoretical results, thereby confirming accuracy of the derived analytical expressions of outage probability. It is observed that the outage probability increases with imperfections in the CSI for both the no-relay and relayed link. Further, considering no-relay case as the benchmark, it is observed that the use of relays significantly improves performance of the system as compared to the no-relay case for both perfect and imperfect channel estimates. As an example, for a target outage probability of 10^{-4}, with $N_r = 2$, an SNR gain of around 19.5 dB is achieved over benchmark case for both the perfect CSI ($\rho \to \infty$) and imperfect CSI ($\rho = 0.1, 0.9$) cases.

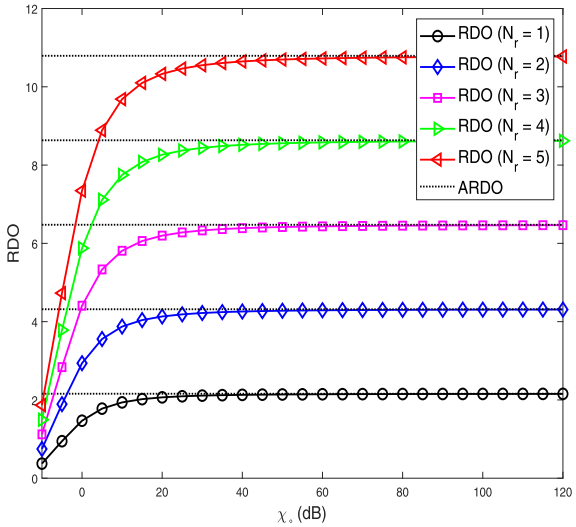

(a) RDO and ARDO versus $\chi_\circ$ for different N_r.

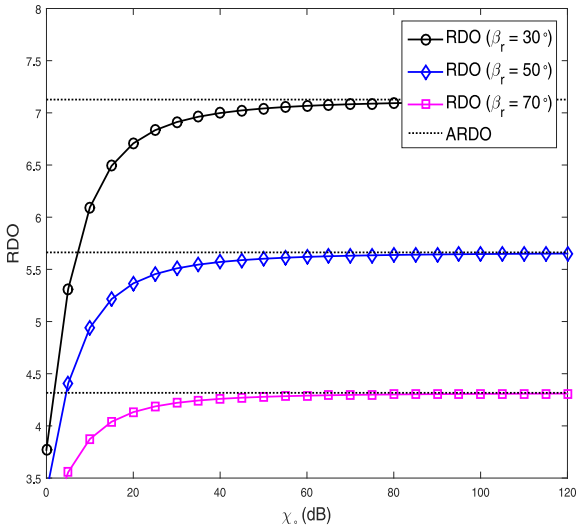

(b) RDO and ARDO versus $\chi_\circ$ for different β_r.

FIGURE 4. RDO and ARDO results for different number of relays and relay elevation angles.

Fig. 3(b) illustrates the outage probability versus relay elevation angle ($\beta_{SR_k} = \beta_{R_kD} = \beta_r$) for $\rho = (0.1, \infty)$ and $N_r = (1, 2, 3, 4)$. It can be seen that irrespective of the value of N_r and ρ, the system performs better for a lower elevation angle. This performance improvement can be attributed to the reduced distance from Tx and Rx to the CV for a lower elevation angle. In Fig. 3(c), theoretical results of outage probability versus Rx FOV angles ($\phi^{Rx}_{SR_k} = \phi^{Rx}_{R_kD} = \phi'$) are presented for different values of N_r and ρ. It is shown that the system performs better for a large value of FOV irrespective of the number of relays and the quality of channel estimation. This is because, with large FOV, more number of photons are received by the Rx, thereby resulting in improved signal quality. This results in significant reduction in the outage probability of the considered system for a given $\chi_\circ$.

Fig. 3(d) presents theoretical results of outage probability versus N_r for different values of C_n^2, considering both perfect CSI and imperfect CSI cases. It is observed that for all the scenarios, the outage probability improves with increase in number of relays. However, the imperfect estimate of the channel severely degrades the system performance and requires more number of relays to achieve the same performance as that of perfect CSI case. As an example, for $C_n^2 = 1 \times 10^{-5}$, and a target outage probability of 10^{-5}, the required number of relays increases by 1.5 times and 1.8 times for $\rho = 0.9$ and $\rho = 0.1$, respectively, when compared to the perfect CSI case. This can be a tradeoff for system designers to increase relays or use more sophisticated computationally complex CSI estimator at the Rx. Further, it is observed that the outage probability of the system increases with C_n^2. This is because, the turbulence scintillation index is directly proportional to the C_n^2, as a result, higher value of C_n^2 increases fading severity and adversely affects the system performance. Furthermore, as an interesting observation, it can be observed that the impact of the increased fading severity becomes worse as the imperfection in the channel estimation increases.

Fig. 4 depicts RDO of the considered system for different configurations. The ARDO is also plotted considering high SNR values for asymptotic analysis. In Fig. 4(a), it is observed that the diversity order of the system improves with the increase in the number of relays. For instance, ARDO of 2.1584, 4.3168, 6.4752, 8.6336, and 10.7919 are obtained for $N_r = 1, 2, 3, 4$ and 5, respectively. The observed asymptotic values coincides with the RDO curves for higher $\chi_\circ$, thereby confirming accuracy of the derived ARDO expression in (25). Fig. 4(b) shows the RDO and ARDO curves for $N_r = 2$ and different β_r values. As an important observation, it can be seen that, for a constant N_r, the RDO of the system significantly improves for lower elevation angles at relay nodes. It is observed that the ARDO of the system comes out to be 7.1272, 5.6626, and 4.3168 for $\beta_r = 30°, 50°$, and $70°$, respectively.

Fig. 5 presents both numerical and simulation results of ASER versus $\chi_\circ$ for different modulation schemes, N_r, and ρ. It is observed that for all cases, analytical results and simulation results closely overlap, thus, validating correctness of the derived ASER analytical expressions. Fig. 5(a) presents comparison of different 32-points RQAM, HQAM, and XQAM constellations for the considered multi-relay case with benchmark system for $N_r = (1, 2)$ and $\rho = 0.1$. It is observed that the use of relays provide significant gain in terms of the required SNR for a target ASER. Considering a target ASER of 10^{-5}, the SNR gains of around 13 dB, 13.14 dB, 13.28 dB, and 13.3 dB are obtained with $N_r = 1$ for RQAM-16 $\times$ 2, RQAM-8$\times$4, XQAM-32, and HQAM-32, respectively, when compared with no-relay case. Further, ASER performance of the system improves significantly by increasing the number of relays. As an example, we observe that for $N_r = 2$,

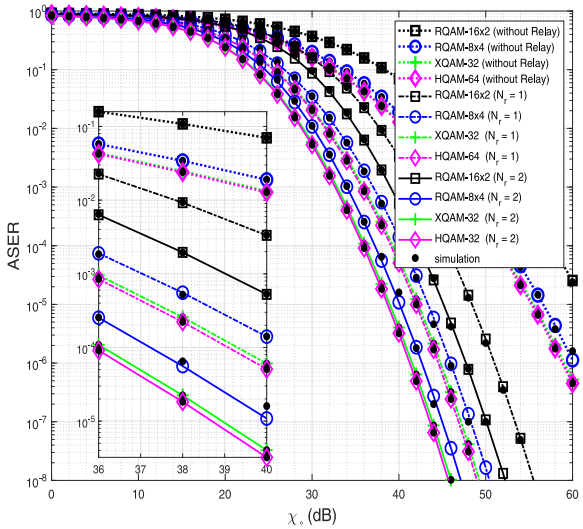

(a) 32-points constellations with comparison to the benchmark system for $N_r = (1, 2)$, and $\rho = 0.1$.

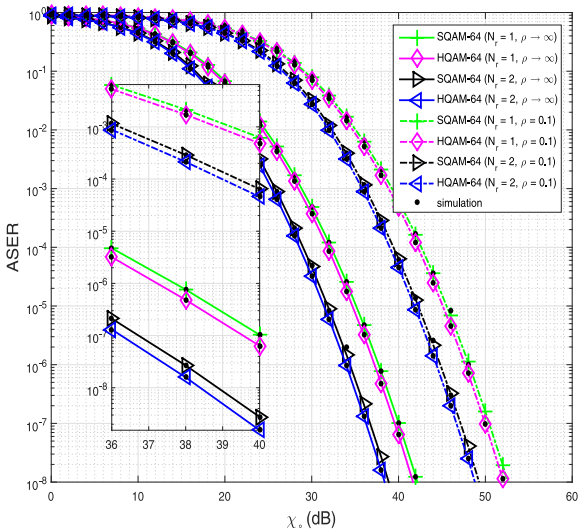

(b) 64-points constellations for $N_r = (1, 2)$, and $\rho = (0.1, \infty)$.

FIGURE 5. Analytical and simulation results of ASER versus SNR for 32-points and 64-points constellations for different QAM schemes.

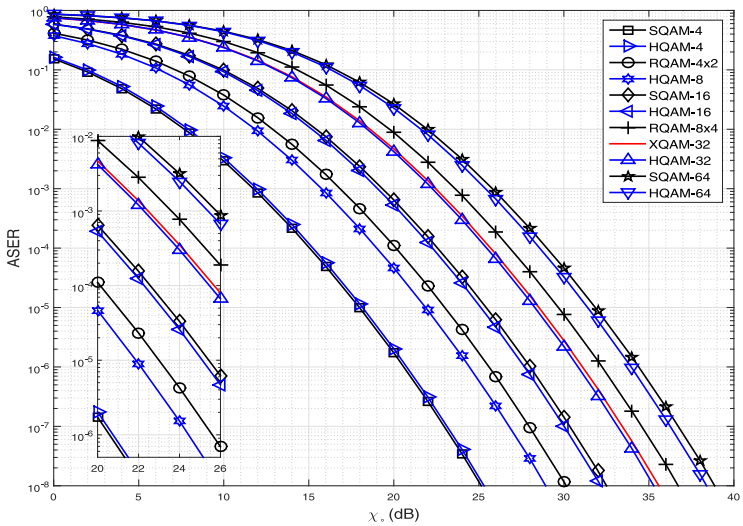

FIGURE 6. Theoretical ASER results for 4, 8, 16, 32, 64-points constellations in perfect CSI conditions and $N_r = 2$.

considerable SNR gains of approximately 3.3 dB, 3.3 dB, 3.1 dB, and 3.2 dB are obtained for RQAM-16 × 2, RQAM-8 × 4, XQAM-32, and HQAM-32, respectively, as compared with $N_r = 1$.

In Fig. 5(b), the ASER performance of SQAM-64 and HQAM-64 constellations are presented for $N_r = (1, 2)$ and $\rho = (0.1, \infty)$. It is observed that HQAM-64 shows better performance as compared to SQAM-64 schemes due to its higher value of q, and low peak and average powers as compared to SQAM. Further, it is observed that irrespective of the selected modulation scheme, the ASER of the system increases as the quality of the channel estimate deteriorates. As an example, to achieve a target ASER of 10^{-5}, for $\rho = 0.1$, HQAM-64 provides a significant gain of 0.4 dB as compared to SQAM-64. Further, using two relays ($N_r = 2$) provides an additional gain of approx. 3.3 dB when compared with single relay ($N_r = 1$) case, due to the improved diversity order.

Fig. 6, illustrates the ASER performance comparison of RQAM, SQAM, XQAM, and HQAM schemes with different constellation points for perfect CSI case and $N_r = 2$. It can be seen that XQAM-32 outperforms RQAM-8 × 4 with a significant gain of 1.1 dB. This is because, XQAM is spectrally more efficient than RQAM for odd number of bits, due to its better peak and average powers as compared to RQAM. It can be seen that, except for HQAM-4, HQAM outperforms SQAM, RQAM, and XQAM irrespective of the number of constellation points. For perfect CSI

case and $N_r = 2$, for ASER of 10^{-5}, HQAM-64 provides approx. 0.4 dB gain over SQAM-64; HQAM-32 provides approx. 0.24 dB gain over XQAM-32; and HQAM-16 provides SNR gain of approx. 0.3 dB over SQAM-16. This performance improvement can be attributed to the optimum placement of constellation points in HQAM as compared to other modulation schemes.

VIII. CONCLUSION

In this paper, we proposed a DF based cooperative NLOS UVC system employing the best relay selection technique. The outage and ASER analysis of the system have been carried out for practical imperfect knowledge of CSI at the Rx. The RDO and ARDO of the system are derived and it is observed that the ARDO of the system improves with the increase in the number of relays. Further, it has been shown that, for a fixed number of relays the diversity order of the system improves for the lower elevation angles at the relay nodes. Novel expressions for the outage probability, and ASER are derived. It has been shown that imperfect CSI downgrades the performance of the considered NLOS UVC system. However, the performance loss due to imperfect CSI can be compensated to an extent by using cooperating relaying techniques. Further, we have shown that the lower elevation angle at the relay, and higher Rx FOV, significantly improves the system performance. As an interesting observation, it has been seen that the impact of imperfect CSI becomes severe as the turbulence severity increases, which results in higher SNR requirements to achieve the target system's performance. Furthermore, it has been observed that the HQAM scheme performs significantly better and is robust than RQAM, SQAM, and XQAM schemes for the same average constellation energy and constellation size in multi-relay UVC systems.

APPENDIX A
PROOF OF THEOREM 1

$$\mathbb{E}\big[g(\chi_{e2e})\big] = \int_0^\infty g(\chi) f_{\chi_{e2e}}(\chi) d\chi. \tag{33}$$

On substituting $f_{\chi_{e2e}}(\chi)$ from (19) into (33) we get

$$\mathbb{E}\big[g(\chi_{e2e})\big] = \mathcal{X}_1 + \mathcal{X}_2, \tag{34}$$

where

$$\mathcal{X}_1 = \frac{N_r}{\sqrt{2\pi}\, 2\sigma_{h_{SR}}\chi} \int_0^\infty g(\chi) \times Q\left(\frac{\ln(\chi) - 2\mu_{h_{RD}} + \ln\left(4\epsilon_{RD} + 4\sigma_{e,RD}^2\right)}{2\sigma_{h_{RD}}}\right) \times \left[1 - Q\left(\frac{\ln(\chi) - 2\mu_{h_{RD}} + \ln\left(4\epsilon_{RD} + 4\sigma_{e,RD}^2\right)}{2\sigma_{h_{RD}}}\right) \times Q\left(\frac{\ln(\chi) - 2\mu_{h_{SR}} + \ln\left(4\epsilon_{SR} + 4\sigma_{e,SR}^2\right)}{2\sigma_{h_{SR}}}\right)\right]^{N_r-1} \times \exp\left(\frac{-\left(\ln(\chi) - 2\mu_{h_{SR}} + \ln\left(4\epsilon_{SR} + 4\sigma_{e,SR}^2\right)\right)^2}{8\sigma_{h_{SR}}^2}\right) d\chi, \tag{35}$$

and

$$\mathcal{X}_2 = \frac{N_r}{\sqrt{2\pi}\, 2\sigma_{h_{RD}}\chi} \int_0^\infty g(\chi) \times Q\left(\frac{\ln(\chi) - 2\mu_{h_{SR}} + \ln\left(4\epsilon_{SR} + 4\sigma_{e,SR}^2\right)}{2\sigma_{h_{SR}}}\right) \times \left[1 - Q\left(\frac{\ln(\chi) - 2\mu_{h_{SR}} + \ln\left(4\epsilon_{SR} + 4\sigma_{e,SR}^2\right)}{2\sigma_{h_{SR}}}\right) \times Q\left(\frac{\ln(\chi) - 2\mu_{h_{RD}} + \ln\left(4\epsilon_{RD} + 4\sigma_{e,RD}^2\right)}{2\sigma_{h_{RD}}}\right)\right]^{N_r-1} \times \exp\left(\frac{-\left(\ln(\chi) - 2\mu_{h_{RD}} + \ln\left(4\epsilon_{RD} + 4\sigma_{e,RD}^2\right)\right)^2}{8\sigma_{h_{RD}}^2}\right) d\chi. \tag{36}$$

On performing change of variable $\xi = [\ln(\chi) - 2\mu_{h_{SR}} + \ln(4\epsilon_{SR} + 4\sigma_{e,SR}^2)]/2\sqrt{2}\,\sigma_{h_{SR}}$ and $\xi = [\ln(\chi) - 2\mu_{h_{RD}} + \ln(4\epsilon_{RD} + 4\sigma_{e,RD}^2)]/2\sqrt{2}\,\sigma_{h_{RD}}$ in (35) and (36), respectively, and after simplification, we get (37) and (38), given on bottom of the next page. Solving (37) and (38) using Gauss-Hermite quadrature integration technique [46, Table 25.10], and substituting the resulting expressions into (34) results in (20).

APPENDIX B
PROOF OF THEOREM 2

In high SNR regime, on substituting the value of $\epsilon_p, p \in \{SD, SR, RD\}$ into (18) and (22), and rearranging the terms, we get

$$P_{out}^{e2e} \approx \left[Q\left(\frac{-\ln(\chi) + 2\mu_{h_{SR}} - \ln\left(4\ell_{SR}^{-2}\right) + \ln(\chi_\circ)}{2\sigma_{h_{SR}}}\right) + Q\left(\frac{-\ln(\chi) + 2\mu_{h_{RD}} - \ln\left(4\ell_{RD}^{-2}\right) + \ln(\chi_\circ)}{2\sigma_{h_{RD}}}\right) - Q\left(\frac{-\ln(\chi) + 2\mu_{h_{SR}} - \ln\left(4\ell_{SR}^{-2}\right) + \ln(\chi_\circ)}{2\sigma_{h_{SR}}}\right) \times Q\left(\frac{-\ln(\chi) + 2\mu_{h_{RD}} - \ln\left(4\ell_{RD}^{-2}\right) + \ln(\chi_\circ)}{2\sigma_{h_{RD}}}\right)\right]^{N_r} \tag{39}$$

and

$$P_{out}^{SD} \approx Q\left(\frac{-\ln(\chi) + 2\mu_{h_{SD}} - \ln\left(4\ell_{SD}^{-2}\right) + \ln(\chi_\circ)}{2\sigma_{h_{SD}}}\right) \tag{40}$$

In (39), the term involving product of two $Q(\cdot)$ functions is negligibly small as compared to other terms, and can safely be ignored for analytical tractability, resulting in

$$P_{out}^{e2e} \approx \left[Q\left(\frac{-\ln(\chi) + 2\mu_{h_{SR}} - \ln\left(4\ell_{SR}^{-2}\right) + \ln(\chi_\circ)}{2\sigma_{h_{SR}}} \right) + Q\left(\frac{-\ln(\chi) + 2\mu_{h_{RD}} - \ln\left(4\ell_{RD}^{-2}\right) + \ln(\chi_\circ)}{2\sigma_{h_{RD}}} \right) \right]^{N_r} \tag{41}$$

On rearranging the terms in (40) and (41), and differentiating $\ln(P_{out}^{e2e})$ and $\ln(P_{out}^{SD})$ with respect to $\ln(\chi_\circ)$, we get (42), shown at the bottom of the page, and

$$\frac{\partial \ln P_{out}^{SD}}{\partial \ln \chi_\circ} = \frac{\exp\left(\frac{-\left(\ln(\chi_\circ) - \ln\left(4\ell_{SD}^{-2}\chi\right) + 2\mu_{h_{SD}}\right)^2}{8\sigma_{h_{SD}}^2} \right)}{2\sqrt{2\pi}\sigma_{h_{SD}} Q\left(\frac{\ln(\chi_\circ) - \ln\left(4\ell_{SD}^{-2}\chi\right) + 2\mu_{h_{SD}}}{2\sigma_{h_{SD}}} \right)}, \tag{43}$$

respectively. On substituting (42) and (43) into (21) and simplifying, we get the RDO expression given in (23).

APPENDIX C
PROOF OF THEOREM 3

The well known upper and lower bounds of Q function are given by [28]

$$\frac{z}{(1+z^2)\sqrt{2\pi}} \exp\left(-z^2/2\right) < Q(z) < \frac{1}{z\sqrt{2\pi}} \exp\left(-z^2/2\right). \tag{44}$$

Using these bounds into (23), and applying squeezing theorem [47] at high SNR, results in

$$\text{ARDO} \approx \lim_{\chi_\circ \to \infty} \frac{\frac{\sigma_{h_{SD}}^2 N_r}{\sigma_{h_{SR}}} \exp\left(\frac{-(\ln \chi_\circ)^2}{8\sigma_{h_{SR}}^2} \right)}{\sigma_{h_{SR}} \exp\left(\frac{-(\ln \chi_\circ)^2}{8\sigma_{h_{SR}}^2} \right) + \sigma_{h_{RD}} \exp\left(\frac{-(\ln \chi_\circ)^2}{8\sigma_{h_{RD}}^2} \right)} + \frac{\frac{\sigma_{h_{SD}}^2 N_r}{\sigma_{h_{RD}}} \exp\left(\frac{-(\ln \chi_\circ)^2}{8\sigma_{h_{RD}}^2} \right)}{\sigma_{h_{SR}} \exp\left(\frac{-(\ln \chi_\circ)^2}{8\sigma_{h_{SR}}^2} \right) + \sigma_{h_{RD}} \exp\left(\frac{-(\ln \chi_\circ)^2}{8\sigma_{h_{RD}}^2} \right)}. \tag{45}$$

Using $e^{-x} = \sum_{i=0}^{\infty} \frac{(-x)^i}{i!}$ in (45) and neglecting higher-order terms. After simplification, we obtain the ARDO expression as given in (25).

$$\mathcal{X}_1 = \frac{N_r}{\sqrt{\pi}} \int_0^\infty g\left(\exp\left(2\sqrt{2}\sigma_{h_{SR}}\xi + 2\mu_{h_{SR}} - \ln\left(4\epsilon_{SR} + 4\sigma_{e,SR}^2\right)\right)\right) \times Q\left(\frac{2\sqrt{2}\sigma_{h_{SR}}\xi + 2\mu_{h_{SR}} - \ln\left(4\epsilon_{SR} + 4\sigma_{e,SR}^2\right) - 2\mu_{h_{RD}} + \ln\left(4\epsilon_{RD} + 4\sigma_{e,RD}^2\right)}{2\sigma_{h_{RD}}} \right) \times \left[1 - Q\left(\sqrt{2}\xi\right) Q\left(\frac{2\sqrt{2}\sigma_{h_{SR}}\xi + 2\mu_{h_{SR}} - \ln\left(4\epsilon_{SR} + 4\sigma_{e,SR}^2\right) - 2\mu_{h_{RD}} + \ln\left(4\epsilon_{RD} + 4\sigma_{e,RD}^2\right)}{2\sigma_{h_{RD}}} \right) \right]^{N_r - 1} \exp\left(-\xi^2\right) d\xi, \tag{37}$$

$$\mathcal{X}_2 = \frac{N_r}{\sqrt{\pi}} \int_0^\infty g\left(\exp\left(2\sqrt{2}\sigma_{h_{RD}}\xi + 2\mu_{h_{RD}} - \ln\left(4\epsilon_{RD} + 4\sigma_{e,RD}^2\right)\right)\right) \times Q\left(\frac{2\sqrt{2}\sigma_{h_{RD}}\xi + 2\mu_{h_{RD}} - \ln\left(4\epsilon_{RD} + 4\sigma_{e,RD}^2\right) - 2\mu_{h_{SR}} + \ln\left(4\epsilon_{SR} + 4\sigma_{e,SR}^2\right)}{2\sigma_{h_{SR}}} \right) \times \left[1 - Q\left(\sqrt{2}\xi\right) Q\left(\frac{2\sqrt{2}\sigma_{h_{RD}}\xi + 2\mu_{h_{RD}} - \ln\left(4\epsilon_{RD} + 4\sigma_{e,RD}^2\right) - 2\mu_{h_{SR}} + \ln\left(4\epsilon_{SR} + 4\sigma_{e,SR}^2\right)}{2\sigma_{h_{SR}}} \right) \right]^{N_r - 1} \exp\left(-\xi^2\right) d\xi, \tag{38}$$

$$\frac{\partial \ln P_{out}^{e2e}}{\partial \ln \chi_\circ} \approx \frac{N_r \left[\frac{1}{2\sigma_{h_{SR}}} \exp\left(\frac{-\left(\ln(\chi_\circ) - \ln\left(4\ell_{SR}^{-2}\chi\right) + 2\mu_{h_{SR}}\right)^2}{8\sigma_{h_{SD}}^2} \right) + \frac{1}{2\sigma_{h_{RD}}} \exp\left(\frac{-\left(\ln(\chi_\circ) - \ln\left(4\ell_{RD}^{-2}\chi\right) + 2\mu_{h_{RD}}\right)^2}{8\sigma_{h_{RD}}^2} \right) \right]}{\sqrt{2\pi} \left[Q\left(\frac{\ln(\chi_\circ) - \ln\left(4\ell_{SR}^{-2}\chi\right) + 2\mu_{h_{SR}}}{2\sigma_{h_{SR}}} \right) + Q\left(\frac{\ln(\chi_\circ) - \ln\left(4\ell_{RD}^{-2}\chi\right) + 2\mu_{h_{RD}}}{2\sigma_{h_{RD}}} \right) \right]} \tag{42}$$

REFERENCES

[1] Z. Xu and B. M. Sadler, "Ultraviolet communications: Potential and state-of-the-art," *IEEE Commun. Mag.*, vol. 46, no. 5, pp. 67–73, May 2008.

[2] A. Vavoulas, H. G. Sandalidis, N. D. Chatzidiamantis, Z. Xu, and G. K. Karagiannidis, "A survey on ultraviolet C-Band (UV-C) communications," *IEEE Commun. Surveys Tuts.*, vol. 21, no. 3, pp. 2111–2133, 3rd Quart., 2019.

[3] H. Kitagawa *et al.*, "Effectiveness of 222-nm ultraviolet light on disinfecting SARS-CoV-2 surface contamination," *Amer. J. Infection Control*, vol. 49, no. 3, pp. 299–301, Mar. 2021.

[4] International Commission on Non-Ionizing Radiation, Protection (ICNIRP), "Guidelines on limits of exposure to ultraviolet radiation of wavelengths between 180 nm and 400 nm (incoherent optical radiation)," *Health Phys.*, vol. 87, no. 2, pp. 171–186, Aug. 2004.

[5] X. Sun *et al.*, "71-Mbit/s ultraviolet-B LED communication link based on 8-QAM-OFDM modulation," *Opt. Exp.*, vol. 25, no. 19, pp. 23267–23274, Sep. 2017.

[6] R. Mitra and V. Bhatia, "Minimum error entropy criterion based channel estimation for massive-MIMO in VLC," *IEEE Trans. Veh. Technol*, vol. 68, no. 1, pp. 1014–1018, Jan. 2019.

[7] R. Mitra and V. Bhatia, "Precoded chebyshev-NLMS-based predistorter for nonlinear LED compensation in NOMA-VLC," *IEEE Trans. Commun.*, vol. 65, no. 11, pp. 4845–4856, Nov. 2017.

[8] M. H. Ardakani, A. R. Heidarpour, and M. Uysal, "Performance analysis of relay-assisted NLOS ultraviolet communications over turbulence channels," *IEEE/OSA J. Opt. Commun. Netw.*, vol. 9, no. 1, pp. 109–118, Jan. 2017.

[9] M. H. Ardakani and M. Uysal, "Relay-assisted OFDM for ultraviolet communications: Performance analysis and optimization," *IEEE Trans. Wireless Commun.*, vol. 16, no. 1, pp. 607–618, Jan. 2017.

[10] S. Arya and Y. H. Chung, "Non-line-of-sight ultraviolet communication with receiver diversity in atmospheric turbulence," *IEEE Photon. Technol. Lett.*, vol. 30, no. 10, pp. 895–898, May 2018.

[11] A. Refaai, M. Abaza, M. S. El-Mahallawy, and M. H. Aly, "Performance analysis of multiple NLOS UV communication cooperative relays over turbulent channels," *Opt. Exp.*, vol. 26, no. 16, pp. 19972–19985, Aug. 2018.

[12] K. K. Garg, P. K. Singya, and V. Bhatia, "Performance analysis of NLOS ultraviolet communications with correlated branches over turbulent channels," *IEEE/OSA J. Opt. Commun. Netw.*, vol. 11, no. 11, pp. 525–535, Nov. 2019.

[13] S. Arya and Y. H. Chung, "Amplify-and-forward multihop non-line-of-sight ultraviolet communication in the gamma-gamma fading channel," *IEEE/OSA J. Opt. Commun. Netw.*, vol. 11, no. 8, pp. 422–436, Aug. 2019.

[14] K. K. Garg, P. Shaik, and V. Bhatia, "Performance analysis of cooperative relaying technique for non-line-of-sight UV communication system in the presence of turbulence," *Opt. Eng.*, vol. 59, no. 5, pp. 1–16, Apr. 2020.

[15] K. K. Garg and V. Bhatia, "Performance analysis of cooperative NLOS UVC system with receiver diversity," in *Proc. Nat. Conf. Commun. (NCC)*, Feb. 2020, pp. 1–6.

[16] M. Seyfi, S. Muhaidat, and J. Liang, "Amplify-and-forward selection cooperation over Rayleigh fading channels with imperfect CSI," *IEEE Trans. Wireless Commun.*, vol. 11, no. 1, pp. 199–209, Jan. 2012.

[17] V. Bhatia, B. Mulgrew, and D. D. Falconer, "Non-parametric maximum-likelihood channel estimator and detector for OFDM in presence of interference," *IET Commun.*, vol. 1, no. 4, pp. 647–654, Aug. 2007.

[18] K. K. Garg, P. Shaik, and V. Bhatia, "On the performance of hybrid RF/NLOS UVC system with imperfect channel estimation (submitted for publication)," *IEEE Trans. Veh. Technol.*, early access.

[19] P. K. Singya, N. Kumar, and V. Bhatia, "Impact of imperfect CSI on ASER of hexagonal and rectangular QAM for AF relaying network," *IEEE Commun. Lett.*, vol. 22, no. 2, pp. 428–431, Feb. 2018.

[20] P. K. Singya, N. Kumar, V. Bhatia, and M.-S. Alouini, "On performance of hexagonal, cross, and rectangular QAM for multi-relay systems," *IEEE Access*, vol. 7, pp. 60602–60616, 2019.

[21] P. Shaik, P. K. Singya, and V. Bhatia, "On impact of imperfect CSI over hexagonal QAM for TAS/MRC-MIMO cooperative relay network," *IEEE Commun. Lett.*, vol. 23, no. 10, pp. 1721–1724, Oct. 2019.

[22] P. Shaik, K. K. Garg, and V. Bhatia, "On impact of imperfect channel state information on dual-hop nonline-of-sight ultraviolet communication over turbulent channel," *Opt. Eng.*, vol. 59, no. 1, pp. 1–14, Jan. 2020.

[23] S. Arnon, J. Barry, G. Karagiannidis, R. Schober, and M. Uysal, *Advanced Optical Wireless Communication Systems*. Cambridge, U.K.: Cambridge Univ. Press, 2012.

[24] X. Song, F. Yang, and J. Cheng, "Subcarrier intensity modulated optical wireless communications in atmospheric turbulence with pointing errors," *IEEE/OSA J. Opt. Commun. Netw.*, vol. 5, no. 4, pp. 349–358, Apr. 2013.

[25] M. Niu, J. Cheng, and J. F. Holzman, "Error rate performance comparison of coherent and subcarrier intensity modulated optical wireless communications," *IEEE/OSA J. Opt. Commun. Netw.*, vol. 5, no. 6, pp. 554–564, Jun. 2013.

[26] M. Z. Hassan, X. Song, and J. Cheng, "Subcarrier intensity modulated wireless optical communications with rectangular QAM," *IEEE/OSA J. Opt. Commun. Netw.*, vol. 4, no. 6, pp. 522–532, Jun. 2012.

[27] P. Shaik, P. K. Singya, and V. Bhatia, "Performance analysis of QAM schemes for non-regenerative cooperative MIMO network with transmit antenna selection," *AEU Int. J. Electron. Commun.*, vol. 107, pp. 298–306, Jul. 2019.

[28] J. G. Proakis and M. Salehi, *Digital Communications*, 5th ed. New York, NY, USA: McGraw-Hill, 2008.

[29] D. Dixit and P. Sahu, "Performance analysis of rectangular QAM with SC receiver over Nakagami-*m* fading channels," *IEEE Commun. Lett.*, vol. 18, no. 7, pp. 1262–1265, Jul. 2014.

[30] X.-C. Zhang, H. Yu, and G. Wei, "Exact symbol error probability of Cross-QAM in AWGN and fading channels," *EURASIP J. Wireless Commun. Netw.*, vol. 2010, no. 1, pp. 1–9, Nov. 2010.

[31] L. Rugini, "Symbol error probability of hexagonal QAM," *IEEE Commun. Lett.*, vol. 20, no. 8, pp. 1523–1526, Aug. 2016.

[32] X. He *et al.*, "Deep UV micro-LED arrays for optical communications," in *Proc. Int. Conf. UV LED Technol. Appl. (ICULTA)*, Apr. 2018, pp. 811–813.

[33] Z. Xu, H. Ding, B. M. Sadler, and G. Chen, "Analytical performance study of solar blind non-line-of-sight ultraviolet short-range communication links," *Opt. Lett.*, vol. 33, no. 16, pp. 1860–1862, Aug. 2008.

[34] Z. Yong, W. Jian, X. Houfei, and L. Jintong, "Non-line-of-sight ultraviolet communication performance in atmospheric turbulence," *China Commun.*, vol. 10, no. 11, pp. 52–57, Nov. 2013.

[35] A. Bucholtz, "Rayleigh-scattering calculations for the terrestrial atmosphere," *Appl. Opt.*, vol. 34, no. 15, pp. 2765–2773, May 1995.

[36] A. S. Zachor, "Aureole radiance field about a source in a scattering—Absorbing medium," *Appl. Opt.*, vol. 17, no. 12, pp. 1911–1922, Jun. 1978.

[37] M. Z. Hassan, M. J. Hossain, J. Cheng, and V. C. Leung, "Subcarrier intensity modulated optical wireless communications: A survey from communication theory perspective," *ZTE Commun.*, vol. 14, no. 2, pp. 2–12, Apr. 2016.

[38] X. Song, F. Yang, J. Cheng, N. Al-Dhahir, and Z. Xu, "Subcarrier phase-shift keying systems with phase errors in lognormal turbulence channels," *J. Lightw. Technol.*, vol. 33, no. 9, pp. 1896–1904, May 2015.

[39] S. Han, S. Ahn, E. Oh, and D. Hong, "Effect of channel-estimation error on BER performance in cooperative transmission," *IEEE Trans. Veh. Technol.*, vol. 58, no. 4, pp. 2083–2088, May 2009.

[40] N. Kumar, P. K. Singya, and V. Bhatia, "ASER analysis of hexagonal and rectangular QAM schemes in multiple-relay networks," *IEEE Trans. Veh. Technol.*, vol. 67, no. 2, pp. 1815–1819, Feb. 2018.

[41] J. Hu and N. C. Beaulieu, "Performance analysis of decode-and-forward relaying with selection combining," *IEEE Commun. Lett.*, vol. 11, no. 6, pp. 489–491, Jun. 2007.

[42] M. Safari and M. Uysal, "Cooperative diversity over log-normal fading channels: Performance analysis and optimization," *IEEE Trans. Wireless Commun.*, vol. 7, no. 5, pp. 1963–1972, May 2008.

[43] G. Pan, E. Ekici, and Q. Feng, "Performance analysis of multi-branch multi-hop wireless relay systems over log-normal channels," *IEEE Trans. Wireless Commun.*, vol. 13, no. 1, pp. 223–233, Jan. 2014.

[44] M. Elamassie, M. Al-Nahhal, R. C. Kizilirmak, and M. Uysal, "Transmit laser selection for underwater visible light communication systems," in *Proc. IEEE 30th Annu. Int. Symp. Pers. Indoor Mobile Radio Commun. (PIMRC)*, Nov. 2019, pp. 1–6.

[45] L. C. Andrews, R. L. Phillips, and C. Y. Hopen, *Laser Beam Scintillation With Applications*, vol. 99. Bellingham, WA, USA: SPIE Press, 2001.
[46] M. Abramowitz and I. A. Stegun, *Handbook of Mathematical Functions*, Nat. Bureau Stand., Washington, DC, USA, Jun. 1972.
[47] F. Caliò and A. Lazzari, *Elements of Mathematics With Numerical Applications*, 2nd ed. New York, NY, USA: Società Editrice Esculapio, 2017.

KAMAL K. GARG received the M.Tech. degree in signal processing from the Netaji Subhash Institute of Technology, New Delhi, India, in 2002. He is currently pursuing the Ph.D. degree from the Indian Institute of Technology Indore, India. He has more than 14 years of industrial experience in satellite mobile communications field. He has also served as a Faculty Member with the Jaypee Institute of Institute Technology, Noida, India, from 2002 to 2007. His research interests include design and performance analysis of wireless communication systems, optical wireless communications, and non-line-of-sight ultraviolet communications.

PARVEZ SHAIK (Graduate Student Member, IEEE) received the B.E. degree in electronics and communication engineering from the YSR Engineering College of Yogi Vemana University, Proddatur, India, in 2012, and the M.Tech. degree in communication systems from the Sri Venkateswara University College of Engineering, Tirupati, India, in 2016. He is currently pursuing the Ph.D. degree from the Indian Institute of Technology Indore, India. His research interest includes design, performance analysis, and optimization of RF and optical wireless cooperative networks over various fading channels.

PRAVEEN K. SINGYA (Member, IEEE) received the B.E. degree in electronics and communication engineering from Jabalpur Engineering College, Jabalpur, India, in 2012, the M.Tech. degree in communication system engineering from VNIT, Nagpur, India, in 2014, and the Ph.D. degree from the Indian Institute of Technology Indore, India, in 2019. He is currently a Postdoctoral Fellow with the King Abdullah University of Science and Technology, Thuwal, Saudi Arabia. His research interest includes design and performance analysis of various wireless networks over different fading channels.

VIMAL BHATIA (Senior Member, IEEE) received the Ph.D. degree from the Institute for Digital Communications, The University of Edinburgh, Edinburgh, U.K., in 2005, U.K., in 2005. He is currently working as a Professor with the Indian Institute of Technology Indore, India. He is also an Adjunct Faculty with IIIT Delhi, India. He has over 200 peer-reviewed publications, book chapters, and filed 11 patents. His research interests include the broader areas of non-Gaussian nonparametric signal processing with applications to communications. During his Ph.D., he received the IEE fellowship for collaborative research on OFDM with Prof. Falconer with the Department of Systems and Computer Engineering, Carleton University, Ottawa, ON, Canada, and the Young Faculty Research Fellow from MeitY. He is also the General Co-Chair for IEEE ANTS 2018, and the General Vice-Chair for IEEE ANTS 2017. He is PI for external funding of over USD 2.0 million. He is a Reviewer for the IEEE, OSA, Elsevier, Wiley, Springer, and IET. He is currently a Fellow of the IETE.